Physical Recognition via Podoplanin is Responsible for the Distinct Blood and Lymphatic Capillaries

Donghyun Jeong[1], Eva Hall[1], Erin Neu[2], Donny Hanjaya-Putra[1,2,3]

[1] Department of Aerospace and Mechanical Engineering, Bioengineering Graduate Program, University of Notre Dame, IN 46556
[2] Department of Chemical and Biomolecular Engineering, University of Notre Dame, IN 46556
[3] Harper Cancer Research Institute, University of Notre Dame, IN 46556

Correspondence to:

Donny Hanjaya-Putra
141 Multidisciplinary Research Building
University of Notre Dame
Notre Dame, IN 46556
Email: dputra1@nd.edu
Phone: 574-631-2291

Abstract

Introduction:

Controlling the formation of blood and lymphatic vasculatures is crucial for engineered tissues. Although the lymphatic vessels originate from embryonic blood vessels, the two retain functional and physiological differences even as they develop in the vicinity of each other. This suggests that there is a previously unknown molecular mechanism by which blood (BECs) and lymphatic endothelial cells (LECs) recognize each other and coordinate to generate distinct capillary networks.

Methods:

We utilized Matrigel and fibrin assays consisting of LECs and BECs to determine how cord-like structures (CLS) can be controlled by altering LEC and BEC identity through podoplanin (*PDPN*) and folliculin (*FLCN*) expressions. We generated $BEC^{\Delta FLCN}$ and $LEC^{\Delta PDPN}$, and observed cell migration to characterize loss lymphatic and blood characteristics due to respective knockouts.

Results:

We observed that LECs and BECs form distinct CLS in Matrigel and fibrin gels despite being cultured in close proximity with each other. We confirmed that the LECs and BECs do not recognize each other through paracrine signaling, as proliferation and migration of both cells were unaffected by paracrine signals. On the other hand, we found *PDPN* as the key surface protein that is responsible for physical LEC-BEC recognition, and LECs lacking *PDPN* became pseudo-BECs and vice versa. We also found that *FLCN* maintains BEC identity through downregulation of *PDPN*.

Conclusions:

Overall, these observations reveal a new molecular pathway through which LECs and BECs form distinct microvascular networks, which has important implications toward designing functional engineered tissues.

Keywords:

Blood Endothelial Cells

Lymphatic Endothelial Cells

Fibrin Hydrogels

Podoplanin

Blood-Lymphatic Separation

Abbreviations:

BECs	Blood Endothelial Cells
CLEC-2	C-type lectin-like receptor 2
CLS	Cord-Like Structures
FLCN	Folliculin
LECs	Lymphatic Endothelial Cells
PDPN	Podoplanin
VEGF	Vascular Endothelial Growth Factor
qRT-PCR reaction	Real time quantitative reverse transcription polymerase chain

Introduction

The lymphatic system is an essential secondary vascular system that is responsible for key functions such as interstitial pressure regulation, immune cell trafficking, and dietary fat absorption.[1,2] Damages to lymphatic vessels are associated with lymphedema, cancer metastasis, and inflammation, showing the importance of lymphatic system to proper tissue function.[3,4] Despite its significance, the lymphatic system has only recently been a subject of investigation with the discovery of markers, such as podoplanin (PDPN), lymphatic vessel endothelial hyaluronan receptor-1 (LYVE-1), prospero-homeobox-1 (Prox1) that distinguish lymphatic endothelial cells (LECs) from that of blood endothelial cells (BECs).[5–7]

Discovering the molecular mechanism that controls angiogenesis and lymphangiogenesis is crucial for the future of tissue engineering.[8–11] Due to limitations of nutrient diffusion, engineered tissues with thickness in any dimension exceeding 400 μm require a vascular system for growth and survival after *in vivo* implantation.[12] While most of the research into vascularized tissue engineering has been focused on blood vessels, addition of lymphatic vessels to engineered tissues has been shown to impart immunological functions to organs and improve their functions.[13] It has been demonstrated that in vascular organoids, lymphatic and blood vessels do not form joined microvasculature.[14] Physiologically, venous and lymphatic vessels use different valve systems, where the venous valve contracts but lymphatic valves contract rhythmically to pump the lymph.[15–17] These incompatibilities indicate that the two cell lines maintain separation and undergo distinct capillary tube formation, but the exact molecular mechanism behind BECs and LECs recognition is yet unclear.

According to the widely accepted venous origin theory, LECs originate from the cardinal vein during embryonic development when venous endothelial cells express adult lymphatic marker LYVE-1 and PDPN.[18,19] The committed LECs express lymphatic markers and master regulator gene *Prox1*, which lead to subsequent divergence of cell lines.[7,20,21] Following lymphatic commitment, the two vessels do not normally form conjoined vessels, but undergo separate capillary tube formation despite developing in the vicinity of each other.[22,23] When BECs and LECs are cultured in a fibrin scaffold, they form separate, distinguishable networks.[24,25] Recently, a tumor suppressor gene called folliculin (*FLCN*) has been identified as a key regulator in maintaining LEC-BEC separation.[26] Inhibiting *FLCN* in BECs causes them to express some LEC-like features and lead to formation of blood-filled lymphatic vessels. Similarly, inhibition of a transmembrane protein called PDPN, one of lymphatic markers responsible for early separation process of LECs from BECs, also results in blood-filled lymphatic vessels in mice.[27–30]

Here, we identify a novel pathway that regulates distinct cord-like networks formation through cell-cell recognition between LEC and BEC. This finding, along with a better understanding of how LECs and BECs interact with different biomaterials, will allow us to exert greater control over development of tissue engineered tissues with functional blood and lymphatic vessels.

Materials and Methods

Human BEC and LEC Culture

Human BECs and LECs derived from the dermis of two adult donors (PromoCell, Heidelberg, Germany) were expanded and used for experiments between passages 5 and 9. Human BECs and LECs were grown in endothelial cell growth medium MV 2 (EGM MV2; PromoCell) incubated at 37°C with 5% CO_2. Human BECs were characterized for the positive expression of CD31 and for the negative expression of Prox-1 and PDPN. Human LECs were characterized for the positive expression of CD31, Prox-1, and PDPN throughout the experiments. All cell lines were routinely tested for mycoplasma contamination and were negative throughout this study.

Migration Assay

To study cell migration, transwell inserts (Falcon™ Cell Culture Inserts 08-771-21, pore size 8μm) were placed into a 24-well plate. 30,000 cells per well were seeded in the top portion of the transwell insert. Migration was stimulated by a 10% FBS gradient added to the bottom of the wells. The transwell plate was incubated at 37°C, 5% CO_2. After a 4hr incubation period, the top part of each transwell was wiped with a cotton swab to remove non-migrated cells. Migrated cells at the bottom of the transwells were fixed with 4% paraformaldehyde for 15 min at 37°C, then washed with PBS. Fixed cells were stained with 1% Crystal Violet in 10% Acetic Acid at room temperature for 10-15 min, then washed with PBS. Seven to eight random areas were imaged per condition and quantified to determine the number of migrated cells in the assay.

Wound Healing Assay

The 2-well culture inserts (ibidi) were placed in each well of a 24-well plate. Cells were seeded inside each chamber and incubated for 24 hours to reach confluence. At this point, the culture inserts were removed to create scratch areas and imaging was initiated (Lionheart FX Automated Microscope, BioTek) to visualize the wound closure process. Wound confluency was measured in 30 min increments for 14 hr. Data was obtained from Gen5 software (BioTek) and was analyzed using GraphPad Prism.

2D Matrigel Assay

To visualize network formation *in vitro*, a Matrigel angiogenesis assay was performed using a 15-well angiogenesis plate (μ-Slide Angiogenesis, ibidi)[31]. Each well was coated with Matrigel and incubated at 37°C for at least 2 hr. Cells were then seeded onto each Matrigel-containing well at a density of 4,000 cells per well. Network formation was visualized and imaged every 30 minutes for 10 hr (Lionheart FX Automated Microscope, BioTek). Analysis was performed using the AutoTube, a freely available MATLAB software that can process a fluorescent image and generate skeletonized outline of the network.[32–34] Data was analyzed using GraphPad Prism.

3D Vasculogenesis Assay

The first layer of fibrin gel was prepared by mixing 30μL of 7 wt% fibrinogen solution with 20μL of thrombin solution provided by Fibrin *In Vitro* Angiogenesis Assay kit (Sigma Aldrich) into each of 96-well plate wells and incubating at 37°C for 20 minutes. Relevant cells were passaged using trypsin/EDTA solution and resuspended into fresh MV2 media containing 100ng/mL of VEGF-C at concentration of 50,000 cells/mL. 100μL

of the cell suspension was added on top of the first layer of the gel and allowed to settle for 24 hours at 37°C. Then the media was aspirated and another layer of 30μL of fibrinogen and 20μL of thrombin solution was added on top of the seeded cells and incubated at 37°C for 5 minutes. Then 100μL of MV2 media containing 100ng/mL of VEGF-C was added to top of the gel. Cells were allowed to form networks for 48 hours, then imaged. Fibrin gels were imaged on the confocal microscope (A1R Nikon) using Texas Red and FITC channels. We captured 31 z-stack images across 200μm along the z-axis centered around the stack with the brightest fluorescence signals as determined visually.

Microvasculature Network Quantification Method

We quantified the vascular network using AutoTube, a freely available MATLAB software that can process a fluorescent image and generate skeletonized outline of the network.[34] For each image, we analyzed each fluorescent channel separately and performed a max-projection across all z steps and adjusted the contrast such that the cells were clearly visible with low background signal. Four parameters per image were quantified, and the tube length and network area were selected to compare the degree of CLS formation. For each hydrogel condition, at least three independent experiments were performed with two technical replicates.

RNAi Transfection

Human BECs or LECs were transfected with siGENOME SMARTpool human *FLCN* or human *PDPN* (Dharmacon, Lafayette, CO) using the manufacturer's protocol. Human BECs or LECs were cultured to 90% confluency in 6-well plates with EGM MV2

media (PromoCell) and no additional VEGF-C supplementation. The RNAi transfection solution was prepared by mixing DharmaFECT2 RNAi transfection reagent (Dharmacon) with serum-free and antibiotic-free EGM MV2 media. To transfect the cells, EGM MV2 media was removed and replaced with 1.6mL of antibiotic-free EGM MV2 and 400µL transfection solution in each well to achieve a final RNAi concentration of 50nM. Transfected cells were incubated at 37°C and 5% CO_2. After 72 hours, total RNA was isolated and real-time qRT-PCR was performed, as described in the previous sub-section, to confirm the knock-down of *FLCN* or *PDPN* expression.

Gene expression

To analyze the gene expressions, BECs or LECs were cultured on hydrogels or tissue culture plastic for 48 hours in their culture media. The 48 hours timepoint was selected to ensure that the signaling cascade in response to VEGF-C and mechanical stimulation was captured. Each biological replicate was created by pooling RNA from three individual wells to collect enough RNA. At least three biological replicates (n=3) were collected per condition and analyzed with real-time qRT-PCR with triplicate readings as previously described.[24,25] RNA was reverse transcribed using a High-Capacity cDNA Reverse Transcription Kit (Thermo Fisher) according to the manufacturer's protocol. cDNA was then used with the TaqMan Universal PCR Master Mix and Gene Expression Assays for *PDPN, FLCN,* and *GAPDH*. Each sample was prepared in triplicate and the relative expression was normalized to *GAPDH* and analyzed using the $^{\Delta\Delta}$Ct method.

Statistical Analysis

Data are presented as mean ± standard deviation, unless otherwise were specified in the figure legends. All statistical analysis was conducted in GraphPad Prism. Statistical comparisons were made using Student's *t* test for paired data, analysis of variance (ANOVA) for multiple comparisons, and with Tukey post hoc analysis for parametric data. Significance levels were set at the following: *p<0.05, **p<0.01, ***p<0.001, ****p<0.0001.

Results

Podoplanin is uniquely expressed by LECs, but not BECs

Since both BECs and LECs were isolated from dermal skin vasculatures,[8,36] the initial study was done to first characterize the unique surface markers specific to blood and lymphatic vasculatures.[5,28] Flow cytometry analysis confirmed that BECs express CD31, but not Podoplanin (**Fig 1A** and **Supplementary Fig 1A**). On the other hand, LECs expressed both CD31 and Podoplanin (**Fig 1B** and **Supplementary Fig 1B**). Further quantification of flow cytometry histograms indicated that 92.7% of BECs were $CD31^+$ and $PDPN^-$ (**Fig 1C** and **D**), while 93.8% of LECs were $CD31^+$ and $PDPN^-$ (**Fig 1E** and **F**). These data suggests that the BECs and LECs were pure population of blood and lymphatic endothelial cells, respectively.

BECs and LECs form distinct cord-like structures

Both BECs and LECs have been shown to form cord-like structures (CLS) in 2D and 3D vasculogenesis assays.[25,36,37] We previously used LECs to study *in vitro* lymphatic CLS induced by VEGF-C and substrate stiffness.[36] Therefore, to investigate

whether BECs and LECs can form capillary networks together or independent with respect to each other, we examined *in vitro* formation of CLS from co-cultures of BECs and LECs. We seeded BECs (pre-labeled in CellTracker™ Red CMTPX) and LECs (pre-labeled in CellTracker™ Green CMFDA) at ratios of 100:0, 80:20, 50:50, 20:80, and 0:100 (BECs:LECs) on 2D Matrigel (**Fig 2A** and **Supplementary Fig 2**). After 12 h, CLS formation was observed in all conditions. Interestingly, we found that BECs and LECs formed CLS independent of each other. We rarely found CLS that was formed by BECs and LECs together (**Supplementary Fig 2**).

To further confirm this observation, we performed 3D vasculogenesis assay using fibrin gels, where endothelial cells have been reported to form capillary networks with lumens.[38,39] To quantify the separation of networks of LECs and BECs, we compared the network formation lengths of fibrin gels containing LECs and BECs of same color and cell type, different color but same cell type, and different color and cell type (**Fig 2B**). After 48 hours of encapsulation, the gels were imaged and the resulting fluorescent channels were quantified separately using MATLAB plugin AutoTube, which can quantify the skeletal length of vascular networks (**Supplementary Fig 3**). Because LECs and BECs form intertwining networks when co-cultured *in vitro*, it is often difficult to visually confirm whether BECs and LECs form distinct networks. Using AutoTube, we confirmed that co-cultures of LECs and BECs labeled two different colors resulting in longer overall skeletal length on a single channel analysis compared to monocultures of LECs and BECs labeled two different colors (**Fig 2C**). This indicates that unlike two-color monoculture, co-culture has continuous networks of cells of one color, which indicates that the LEC and BEC networks remain distinct. We also observed no significant difference between network

lengths of co-culture and monoculture with same color (**Fig 2D**), again indicating that LEC and BEC networks consist mostly of the same cell type even in co-cultures.

Paracrine signaling is not responsible for distinct CLS formation

We then explored the possibility of paracrine signaling as a mechanism behind LEC-BEC recognition to form distinct CLS.[40,41] LECs and BECs release a distinct set of paracrine signals which have been implicated in promoting growth of other tissues.[41,42] To collect the paracrine signals, BECs and LECs were cultured in fresh MV2 media for 2 days, and the resulting media was collected and filtered (**Fig 3A**). We performed cell proliferation assay of BECs and LECs when cultured in either conditioned media from BECs or LECs. We used label-free cell counting protocol of Lionheart FX Automated Microscope, which uses brightfield channel to count the number of cells at various timepoints (**Fig 3B** and **C**). We compared the growth rate at around 3500 cells/well and found no significant differences between the two media types (**Fig 3D**).

Furthermore, we performed a trans-well migration assay to test if the paracrine signals from BEC and LEC inhibit cell migration of the opposing cell line, where either media from the same or different cell line was placed in the outer well and cells were allowed to migrate across the bottom membrane (**Fig 3E**). We found no significant differences in migration rate towards the media of same and different cell line, indicating that paracrine signaling is not responsible for affecting cell migration of BECs and LECs (**Fig 3F** and **Supplementary Fig 4**). Collectively, these results suggest that the LECs and BECs do not maintain CLS separation through paracrine signals.

Podoplanin is responsible for distinct CLS formation *in vitro*

To determine if the recognition mechanism is through surface receptors, we tested the effect of Podoplanin on network separation. Previous studies have reported that Folliculin (FLCN) is responsible for BEC-LEC separation by downregulating *Prox1*, a master gene of LEC marker expression, in BECs.[26] Since *PDPN* is one of the key markers of LEC, we hypothesized that BECs downregulate *PDPN* through *FLCN* expression, which allows BECs and LECs to recognize cells of the same lineage through membrane receptor *PDPN*. We generated LEC$^{\Delta PDPN}$ and BEC$^{\Delta FLCN}$ (denoted as ΔLEC and ΔBEC in the figures, respectively) through RNAi transfection. We performed quantitative PCR to confirm that RNAi-*PDPN* reduces *PDPN* expression by at least 90% in both LECs and BECs (**Supplementary Fig 5**). RNAi-*FLCN* transfection increased *PDPN* expression in BECs by twofold, but did not have significant result in *PDPN* expression in LECs, possibly due to already high levels of *PDPN* expression in LECs as confirmed in previous FACS data (**Fig 1G**).

Then, we performed vasculogenesis assay on 3D fibrin gels using LECs and BECs labeled with green or red membrane dyes. Each condition consisted of either green-labeled LEC or LEC$^{\Delta PDPN}$ and red-labeled BEC or BEC$^{\Delta FLCN}$ and imaged after 48 hours under same conditions as previous fibrin gel assay (**Fig 4A-D**). The results were quantified using AutoTube as previously described, and the results were quantified along with LEC-LEC, BEC-BEC, and LEC-BEC data from before. We quantified LECs on the green channel and BECs on the red channel and measured the skeleton length of each network (**Supplementary Fig 3**). We found that knockouts of LECs (**Fig 4B** and **D**) and BECs (**Fig 4C** and **D**) failed to form networks by themselves and resulted in significantly

shorter networks than same-color monoculture (**Fig 4E** and **F**). This indicates that the presence or lack of *PDPN* is crucial for BEC and LEC self-recognition and network formation. Comparatively, when wild-type cells were co-cultured with knockout cells, the network forming capabilities of the non-knockout cell line was not affected (**Fig 4E** and **F**), which may indicate that these new knockout cells are also not being integrated into the network of the other cell line.

Podoplanin is responsible for the BEC and LEC recognition

To fully confirm that LECs and BECs do not avoid BEC$^{\Delta FLCN}$ and LEC$^{\Delta PDPN}$ respectively, we performed wound healing assay to study how cell-cell contact affects cell migration for LEC and BEC. We used an ibidi two-well insert attached to a tissue culture plastic surface, with cells seeded on both wells stained with either the red or green membrane dyes. The conditions we tested were: LEC and LEC, BEC and BEC, LEC and BEC, BEC$^{\Delta FLCN}$ and LEC, and LEC$^{\Delta PDPN}$ and BEC (**Fig 5A-E** and **Supplementary Movie 1-5**). We seeded the cells and allowed them to adhere for 24 hours, then we removed the insert and imaged the wound every hour for 48 hours. The wound was fully closed around 24 hours, and there was no significant difference in the wound closure time. However, we observed that in the LEC-BEC condition (**Fig 5C** and **Supplementary Movie 3**), the cells appeared to change directions when first coming into contact with the other cell line, which resulted in a clear boundary between the two cell lines compared to BEC-BEC (**Fig 5A** and **Supplementary Movie 1**) or BEC-BEC (**Fig 5B** and **Supplementary Movie 2**) conditions.

We hypothesized that when LECs and BECs recognize the other cell line through presence or lack of *PDPN*, they change the direction of movement such that cells of the same lineage group together, which may be the mechanism behind how LECs and BECs form separate vessels *in vivo* even in close proximity with each other. To quantify this, we divided each segment of the wound into smaller segments and generated a density plot for the number of cells across the distance of the wound. Then we used the overlap package in R to estimate the overlap scores in the two density plots. We observed that LECs and BECs do not mix in the middle, as shown by the lower overlap score (**Fig 5F**). This effect is reversed when either the LEC or BEC is replaced with $LEC^{\Delta PDPN}$ or $BEC^{\Delta FLCN}$, which suggests that the knockouts of *PDPN* and *FLCN* in LEC and BEC, respectively, avoids being recognized as the different cell type by BEC and LEC (**Fig 5G**). This indicates that the LEC-BEC recognition mechanism is through cell-cell contact through transmembrane protein *PDPN*.

Discussion

Vascular tissue engineering is critical to the future of transplantable organ engineering as it has the potential to produce microvascular network that can overcome the diffusion limits in non-vascularized organoids.[43,44] Consequently, multiple studies have focused on developing microvasculature networks in various hydrogels, including PLGA, PEG, and hyaluronic acid (HA)-hydrogels.[11,36,45] Fibrin, a wound healing protein, is of particular interest in designing 3D hydrogels to promote vasculogenesis.[46,47] Fibrin is compatible with recapitulating *in vivo* functionalities of both BECs and LECs and therefore has been used in microfluidic devices for LEC-BEC co-culturing to study how

the two cell lines interact.[48–50] Microvasculature engineering in organoids mostly rely on self-assembly of endothelial cells in hydrogels due to the extremely small size of these vessels, which relies on controlling molecular and biomechanical factors to direct network formation.[8,51,52] To our knowledge, there are no studies thus far that explored the molecular mechanism behind LEC and BEC interaction in co-culture at a microvasculature level.

Multiple studies have explored the possible molecular pathways behind lymphatic and blood vessel separation pathways and identified numerous genes involved in this process,[27,28,54,55] but none have identified a unifying pathway that explained how LECs and BECs only join vessels with the same type of cell during *in vivo* embryonic development or *in vitro* angiogenesis in hydrogels. In this study, we explored the molecular mechanism behind the widely reported LEC and BEC tendency to form distinct networks. Previous work has suggested the role of *PDPN* in preventing the mixing of the lymph and the blood through intermittent platelet aggregation near the lymphatic valve.[28,56] *PDPN* is a well-conserved, mucin-type transmembrane protein that can interact with C-type lectin-like receptor 2 (CLEC-2) expressing platelets.[30,54] *FLCN* was also identified as a gene that maintains separation between the lymph and the blood through inhibition of *Prox1* in BECs.[26] We have shown that microvasculature formation in fibrin gels by LECs and BECs can be manipulated through regulation of *FLCN* and *PDPN*. Our study suggests that *PDPN* plays a role in contact-based endothelial cell recognition and capillary formation in addition to lymphatic valve control. Furthermore, we show that the downstream mechanism of *FLCN*-based LEC and BEC physical recognition is through

the inhibition of *PDPN* expression, and that this LEC and BEC identity can be reversed by controlling *PDPN* or *FLCN* expression respectively.

Overall, our results indicate a novel cell-cell contact-based pathway for BECs and LECs to form distinct networks, which can be used to exert a higher degree of control over microvasculature assembly in vascular engineered tissues. This study suggests that *FLCN* and *PDPN* may be responsible for the BECs and LECs plasticity found in the zebrafish, rat mesentery, and human pluripotent stem cells.[23,26,57] Future studies could further elucidate the role of *PDPN* in lymphangiogenesis during embryonic development and the initial separation of LECs from the blood vessels. In clinical applications, *FLCN* deficiency is associated with Birt-Hogg-Dubé syndrome and may contribute to abnormal lymph nodes as well.[26,58] These findings may lead to improved understanding of the effects of *FLCN*-related diseases on lymphatics, which may translate to novel therapeutic approaches to lymphatic disorders.

Acknowledgments

We acknowledge support from the University of Notre Dame through “Advancing Our Vision” Initiative in Stem Cell Research, Harper Cancer Research Institute – American Cancer Society Institutional Research Grant (IRG-17-182-04), American Heart Association through Career Development Award (19-CDA-34630012 to D.H.-P.), and National Science Foundation (2047903 to D.H.-P.). We would like to thank the Notre Dame Integrated Imaging Facility for performing fluorescent imaging.

Conflict of interest statement:

The authors have declared that no conflict of interest exists

Author contributions: D.J. and D.H.-P. conceived the ideas, designed the experiments, interpreted the data, and wrote the manuscript. E.H. and E.N. conducted the experiments and analyzed the data. All authors have approved the manuscript.

Data and materials availability: Additional material and data which contributed to this study are present in the **Supplementary Information**.

Figure Legends

Figure 1. BECs and LECs express unique endothelial surface markers. Representative flow cytometry diagrams demonstrating unique endothelial surface markers for PDPN and CD31. **(A)** BEC (92.7%) showing $CD31^+$ and $PDPN^-$, while **(B)** LEC showing $CD31^+$ and $PDPN^+$. Representative flow cytometry histograms indicating **(C** and **D)** BEC and **(E** and **F)** LEC stained with CD31-PE (in *black*), PDPN-FITC (in *black*), and isotype controls (in *grey*). **(G)** Real-time quantitative qRT-PCR was used to analyze *PDPN* expression for LEC and BEC relative to *GAPDH*. Data represents mean $\pm$ SD, n=4 per group, ***P<0.001. All P values were determined by unpaired t tests.

Figure 2. BEC and LEC form distinct cord-like structures on 2D Matrigel and 3D fibrin gel assays. (A) BEC (pre-labeled in pre-labeled in CellTracker™ Red CMTPX) and LEC (pre-labeled in CellTracker™ Green CMFDA) were seeded on 2D Matrigel at ratios of 100:0, 80:20, 50:50, 20:80, and 0:100 (BECs:LECs). Representative images of cord-like structures (CLS) formation were imaged at 12 hrs. Scale bars are 500 μm. **(B)** BEC and LEC were encapsulated in 3D fibrin gel assay. From left to right, red-BEC only, red-BEC and green-BEC (50:50), red-BEC and green-LEC (50:50), red-LEC and green-LEC (50:50), and green-LEC only. Representative images of CLS formation were imaged at 48 hrs. Scale bars are 500 μm. CLS formed on 3D fibrin gel was quantified for tube length using AutoTube for **(C)** BEC and **(D)** LEC. Data represents mean $\pm$ SD, n=4 per group, n.s. P > 0.05, *P<0.05. All P values were determined by unpaired t tests.

Figure 3. The effects of paracrine signaling on BEC and LEC. (A) A timeline for BEC and LEC-conditioned media collection. Conditioned media were collected after 48 hours of BEC or LEC cultures. Cell proliferation assay with **(B)** BEC and **(C)** LEC using the same (circle data points) and different (square data points) cell line-conditioned media. **(D)** Cell growth rates of BEC and LEC were quantified at 3,500 cells/well using the label-free cell proliferation protocol (Lionheart FX Microscope). Each sample was repeated 12 times. **(E)** A schematic diagram to illustrate the layout of the transwell migration assay. The outer well was filled with conditioned media from either the same or different cell type. **(F)** The top of the membrane was cleaned and imaged on a fluorescence channel to quantify the migrated cells after 24 hours. Each sample was repeated 3 times. Data represents mean $\pm$ SD, n=4 per group, n.s. P > 0.05, All P values were determined by unpaired t tests.

Figure 4. The roles of *FLCN* and *PDPN* on cord-like networks formation. (A and **B)** *Luciferase* knockout BEC (rBEC $^{\Delta Luc}$) or **(C** and **D)** *FLCN* knockout BEC (rBEC$^{\Delta FLCN}$) stained in red are encapsulated in 3D fibrin gels together with **(A** and **C)** *Luciferase* knockout LEC (gLEC $^{\Delta Luc}$) or **(B** and **D)** *PDPN* knockout LEC (rLEC$^{\Delta PDPN}$) stained in green. Representative images of CLS formation were imaged at 48 hrs. Scale bars are 500 μm. **(E** and **F)** CLS formed on 3D fibrin gel was quantified for tube length using AutoTube. Data represents mean $\pm$ SD, n=4 per group, n.s. $P > 0.05$, *$P<0.05$. All P values were determined by unpaired t tests.

Figure 5. The roles of *FLCN* and *PDPN* on cell migration. Representative images of the wound healing assay taken at t=16, 35, and 48 hours for **(A)** BEC (in *red*) : BEC (in *green*), **(B)** LEC $^{\Delta Luc}$ (in *red*) : LEC $^{\Delta Luc}$ (in *green*), **(C)** BEC $^{\Delta Luc}$ (in *red*) : LEC $^{\Delta Luc}$ (in *green*), **(D)** BEC$^{\Delta FLCN}$ (in *red*) : LEC $^{\Delta Luc}$ (in *green*), and **(E)** BEC$^{\Delta FLCN}$ (in *red*) : LEC $^{\Delta Luc}$ (in *green*). Each well was seeded with 7,000 cells and allowed to settle for 24 hours, then imaged for up to 48 hours. Scale bars are 500 μm. Overlap scores for **(F)** wild-type BEC and LEC, as well as **(G)** knock-out BEC and LEC. The LEC-BEC condition consists of 4 replicates and the same and knockout conditions consist of 4 replicates from either of the two conditions. Data represents mean $\pm$ SD, n=4 per group, n.s. $P > 0.05$, *$P<0.05$, **$P<0.01$, and ***$P<0.001$. All P values were determined by unpaired t tests.

References

1. Cueni LN, Detmar M. The Lymphatic System in Health and Disease. *Lymphatic Research and Biology*. 2008;6(3–4):109–122.
2. Oliver G, Kipnis J, Randolph GJ, Harvey NL. The Lymphatic Vasculature in the 21st Century: Novel Functional Roles in Homeostasis and Disease. *Cell*. 2020;182(2):270–296.
3. Alitalo K, Carmeliet P. Molecular mechanisms of lymphangiogenesis in health and disease. *Cancer Cell*. 2002;1(3):219–227.
4. Stritt S, Koltowska K, Mäkinen T. Homeostatic maintenance of the lymphatic vasculature. *Trends in Molecular Medicine*. 2021;27(10):955–970.
5. Wigle JT, Oliver G. Prox1 Function Is Required for the Development of the Murine Lymphatic System. *Cell*. 1999;98(6):769–778.
6. Banerji S, Ni J, Wang S-X, et al. LYVE-1, a New Homologue of the CD44 Glycoprotein, Is a Lymph-specific Receptor for Hyaluronan. *The Journal of Cell Biology*. 1999;144(4):789 LP – 801.
7. Hong Y-K, Harvey N, Noh Y, et al. Prox1 is a master control gene in the program specifying lymphatic endothelial cell fate. *Dev Dyn*. 2002;225(1):351–357.
8. Hanjaya-Putra D, Bose V, Shen Y-I, et al. Controlled activation of morphogenesis to generate a functional human microvasculature in a synthetic matrix. *Blood*. 2011;118(3):804 LP – 815.
9. Alderfer L, Wei A, Hanjaya-Putra D. Lymphatic Tissue Engineering and Regeneration. *Journal of Biological Engineering*. 2018;12(1):32.
10. Henderson AR, Ilan IS, Lee E. A bioengineered lymphatic vessel model for studying lymphatic endothelial cell-cell junction and barrier function. *Microcirculation*. 2021;28(8):e12730.
11. Landau S, Newman A, Edri S, et al. Investigating lymphangiogenesis in vitro and in vivo using engineered human lymphatic vessel networks. *Proc Natl Acad Sci U S A*. 2021;118(31):e2101931118.
12. Auger FA, Gibot L, Lacroix D. The Pivotal Role of Vascularization in Tissue Engineering. *Annu. Rev. Biomed. Eng.* 2013;15(1):177–200.
13. Matsumoto M, Fu Y-X, Molina H, Chaplin D. Lymphotoxin-a-deficient and TNF receptor-I-deficient mice define developmental and functional characteristics of germinal centers. *Immunol Rev*. 1997;156(1):137–144.
14. Abtahian F, Guerriero A, Sebzda E, et al. Regulation of blood and lymphatic vascular separation by signaling proteins SLP-76 and Syk. *Science*. 2003;299(5604):247–251.
15. Hitchcock T, Niklason L. Lymphatic Tissue Engineering. *Annals of the New York Academy of Sciences*. 2008;1131(1):44–49.
16. Breslin JW, Yang Y, Scallan JP, et al. Lymphatic Vessel Network Structure and Physiology. *Compr Physiol*. 2018;9(1):207–299.
17. Mukherjee A, Hooks J, Nepiyushchikh Z, Dixon JB. Entrainment of Lymphatic Contraction to Oscillatory Flow. *Sci Rep*. 2019;9(1):5840–5840.
18. Bautch VL, Caron KM. Blood and Lymphatic Vessel Formation. *Cold Spring Harb Perspect Biol*. 2015;7(3):a008268.

19. Oliver G. Lymphatic vasculature development. *Nat Rev Immunol*. 2004;4(1):35–45.
20. Petrova T, Makinen T, Makela T, et al. Lymphatic endothelial reprogramming of vascular endothelial cells by the Prox-1 homeobox transcription factor. *EMBO J*. 2002;21(17):4593–4599.
21. Oliver G, Srinivasan RS. Endothelial cell plasticity: how to become and remain a lymphatic endothelial cell. *Development*. 2010;137(3):363–372.
22. Jussila L, Alitalo K. Vascular Growth Factors and Lymphangiogenesis. *Physiological Reviews*. 2002;82(3):673–700.
23. Robichaux JL, Tanno E, Rappleye JW, et al. Lymphatic/Blood endothelial cell connections at the capillary level in adult rat mesentery. *Anat Rec (Hoboken)*. 2010;293(10):1629–1638.
24. Knezevic L, Schaupper M, Mühleder S, et al. Engineering Blood and Lymphatic Microvascular Networks in Fibrin Matrices. *Front. Bioeng. Biotechnol.* 2017;5:.
25. Helm C-L, Zisch A, Swartz M. Engineered blood and lymphatic capillaries in 3-D VEGF-fibrin-collagen matrices with interstitial flow. *Biotechnology and Bioengineering*. 2007;96(1):167–176.
26. Tai-Nagara I, Hasumi Y, Kusumoto D, et al. Blood and lymphatic systems are segregated by the FLCN tumor suppressor. *Nat Commun*. 2020;11(1):6314.
27. Bianchi R, Russo E, Bachmann SB, et al. Postnatal Deletion of Podoplanin in Lymphatic Endothelium Results in Blood Filling of the Lymphatic System and Impairs Dendritic Cell Migration to Lymph Nodes. *ATVB*. 2017;37(1):108–117.
28. Uhrin P, Zaujec J, Breuss JM, et al. Novel function for blood platelets and podoplanin in developmental separation of blood and lymphatic circulation. *Blood*. 2010;115(19):3997–4005.
29. Fu J, Gerhardt H, McDaniel JM, et al. Endothelial cell O-glycan deficiency causes blood/lymphatic misconnections and consequent fatty liver disease in mice. *J. Clin. Invest.* 2008;118(11):3725–3737.
30. Bertozzi CC, Schmaier AA, Mericko P, et al. Platelets regulate lymphatic vascular development through CLEC-2–SLP-76 signaling. *Blood*. 2010;116(4):661–670.
31. Vo E, Hanjaya-Putra D, Zha Y, Kusuma S, Gerecht S. Smooth-Muscle-Like Cells Derived from Human Embryonic Stem Cells Support and Augment Cord-Like Structures In Vitro. *Stem Cell Reviews and Reports*. 2010;6(2):237–247.
32. Varberg KM, Winfree S, Chu C, et al. Kinetic analyses of vasculogenesis inform mechanistic studies. *American Journal of Physiology - Cell Physiology*. 2017;
33. Schindelin J, Arganda-Carreras I, Frise E, et al. Fiji: An open-source platform for biological-image analysis. *Nature Methods*. 2012;
34. Montoya-Zegarra JA, Russo E, Runge P, et al. AutoTube: a novel software for the automated morphometric analysis of vascular networks in tissues. *Angiogenesis*. 2019;22(2):223–236.
35. Hanjaya-Putra D, Bose V, Shen Y-I, et al. Controlled activation of morphogenesis to generate a functional human microvasculature in a synthetic matrix. *Blood*. 2011;118(3):804 LP – 815.
36. Alderfer L, Russo E, Archilla A, Coe B, Hanjaya-Putra D. Matrix stiffness primes lymphatic tube formation directed by vascular endothelial growth factor-C. *The FASEB Journal*. 2021;35(5):e21498.

37. Hanjaya-Putra D, Yee J, Ceci D, et al. Vascular endothelial growth factor and substrate mechanics regulate in vitro tubulogenesis of endothelial progenitor cells. *Journal of Cellular and Molecular Medicine*. 2010;14(10):2436–2447.
38. Chen X, Aledia AS, Ghajar CM, et al. Prevascularization of a Fibrin-Based Tissue Construct Accelerates the Formation of Functional Anastomosis with Host Vasculature. *Tissue Engineering Part A*. 2008;15(6):1363–1371.
39. Campbell KT, Hadley DJ, Kukis DL, Silva EA. Alginate hydrogels allow for bioactive and sustained release of VEGF-C and VEGF-D for lymphangiogenic therapeutic applications. *PLOS ONE*. 2017;12(7):e0181484.
40. Lee E, Fertig EJ, Jin K, et al. Breast cancer cells condition lymphatic endothelial cells within pre-metastatic niches to promote metastasis. *Nature Communications*. 2014;5:4715.
41. Liu X, De la Cruz E, Gu X, et al. Lymphoangiocrine signals promote cardiac growth and repair. *Nature*. 2020;588(7839):705–711.
42. Rafii S, Butler JM, Ding B-S. Angiocrine functions of organ-specific endothelial cells. *Nature*. 2016;529(7586):316–325.
43. Chang WG, Niklason LE. A short discourse on vascular tissue engineering. *npj Regen Med*. 2017;2(1):7.
44. Hanjaya-Putra D, Bose V, Shen Y-I, et al. Controlled activation of morphogenesis to generate a functional human microvasculature in a synthetic matrix. *Blood*. 2011;118(3):804 LP – 815.
45. Alderfer L, Hall E, Hanjaya-Putra D. Harnessing biomaterials for lymphatic system modulation. *Acta Biomaterialia*. 2021;133:34–45.
46. Rao RR, Peterson AW, Ceccarelli J, Putnam AJ, Stegemann JP. Matrix composition regulates three-dimensional network formation by endothelial cells and mesenchymal stem cells in collagen/fibrin materials. *Angiogenesis*. 2012;15(2):253–264.
47. Grainger SJ, Carrion B, Ceccarelli J, Putnam AJ. Stromal Cell Identity Influences the In Vivo Functionality of Engineered Capillary Networks Formed by Co-delivery of Endothelial Cells and Stromal Cells. *Tissue Engineering Part A*. 2012;19(9–10):1209–1222.
48. Greenlee JD, King MR. Engineered fluidic systems to understand lymphatic cancer metastasis. *Biomicrofluidics*. 2020;14(1):011502.
49. Smith Q, Gerecht S. Going with the flow: microfluidic platforms in vascular tissue engineering. *Curr Opin Chem Eng*. 2014;3:42–50.
50. Osaki T, Sivathanu V, Kamm RD. Engineered 3D vascular and neuronal networks in a microfluidic platform. *Scientific Reports*. 2018;8(1):5168.
51. Smith Q, Chan XY, Carmo AM, et al. Compliant substratum guides endothelial commitment from human pluripotent stem cells. *Sci Adv*. 2017;3(5):e1602883–e1602883.
52. Abaci HE, Shen Y-I, Tan S, Gerecht S. Recapitulating physiological and pathological shear stress and oxygen to model vasculature in health and disease. *Scientific Reports*. 2014;4:4951.
53. Kim S, Kim W, Lim S, Jeon J. Vasculature-On-A-Chip for In Vitro Disease Models. *Bioengineering*. 2017;4(4):8.

54. Osada M, Inoue O, Ding G, et al. Platelet activation receptor CLEC-2 regulates blood/lymphatic vessel separation by inhibiting proliferation, migration, and tube formation of lymphatic endothelial cells. *Journal of Biological Chemistry*. 2012;
55. Frye M, Taddei A, Dierkes C, et al. Matrix stiffness controls lymphatic vessel formation through regulation of a GATA2-dependent transcriptional program. *Nature Communications*. 2018;9(1):1511.
56. Schacht V, Ramirez MI, Hong Y-K, et al. T1α/podoplanin deficiency disrupts normal lymphatic vasculature formation and causes lymphedema. *The EMBO Journal*. 2003;22(14):3546–3556.
57. Nicenboim J, Malkinson G, Lupo T, et al. Lymphatic vessels arise from specialized angioblasts within a venous niche. *Nature*. 2015;522:56.
58. Dong L, Gao M, Hao W, et al. Case Report of Birt–Hogg–Dubé Syndrome: Germline Mutations of FLCN Detected in Patients With Renal Cancer and Thyroid Cancer. *Medicine*. 2016;95(22):e3695.

Figure Legends

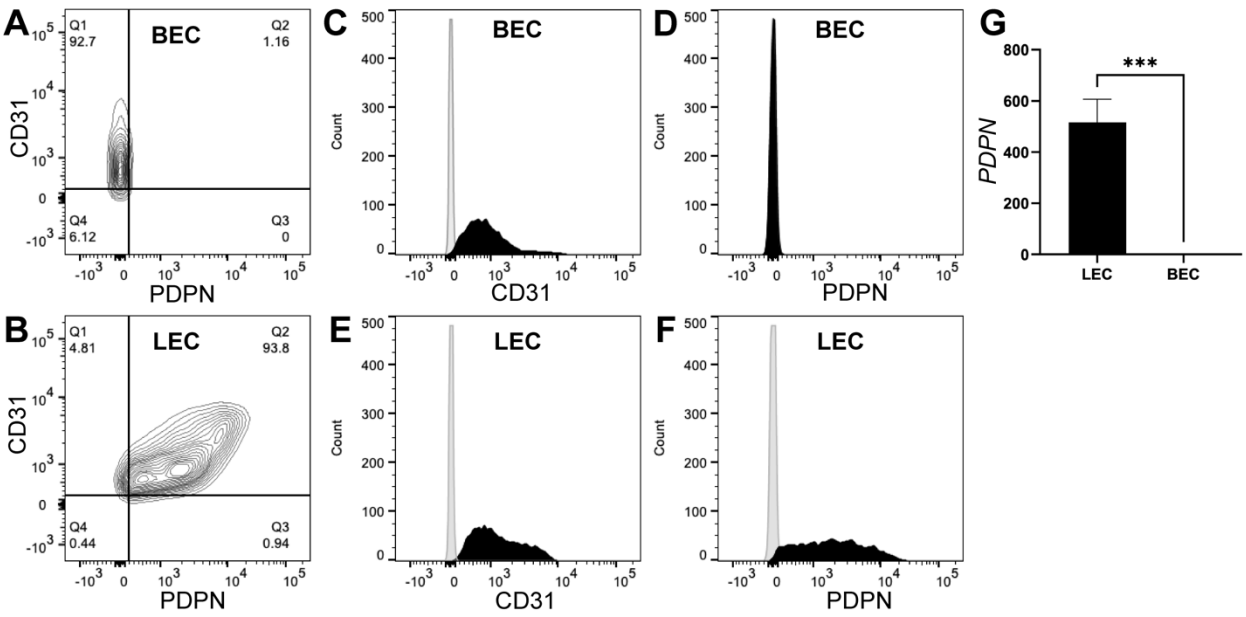

Figure 1. BECs and LECs express unique endothelial surface markers. Representative flow cytometry diagrams demonstrating unique endothelial surface markers for PDPN and CD31. **(A)** BEC (92.7%) showing $CD31^+$ and $PDPN^-$, while **(B)** LEC showing $CD31^+$ and $PDPN^+$. Representative flow cytometry histograms indicating **(C** and **D)** BEC and **(E** and **F)** LEC stained with CD31-PE (in *black*), PDPN-FITC (in *black*), and isotype controls (in *grey*). **(G)** Real-time quantitative qRT-PCR was used to analyze *PDPN* expression for LEC and BEC relative to *GAPDH*. Data represents mean $\pm$ SD, n=4 per group, ***P<0.001. All P values were determined by unpaired t tests.

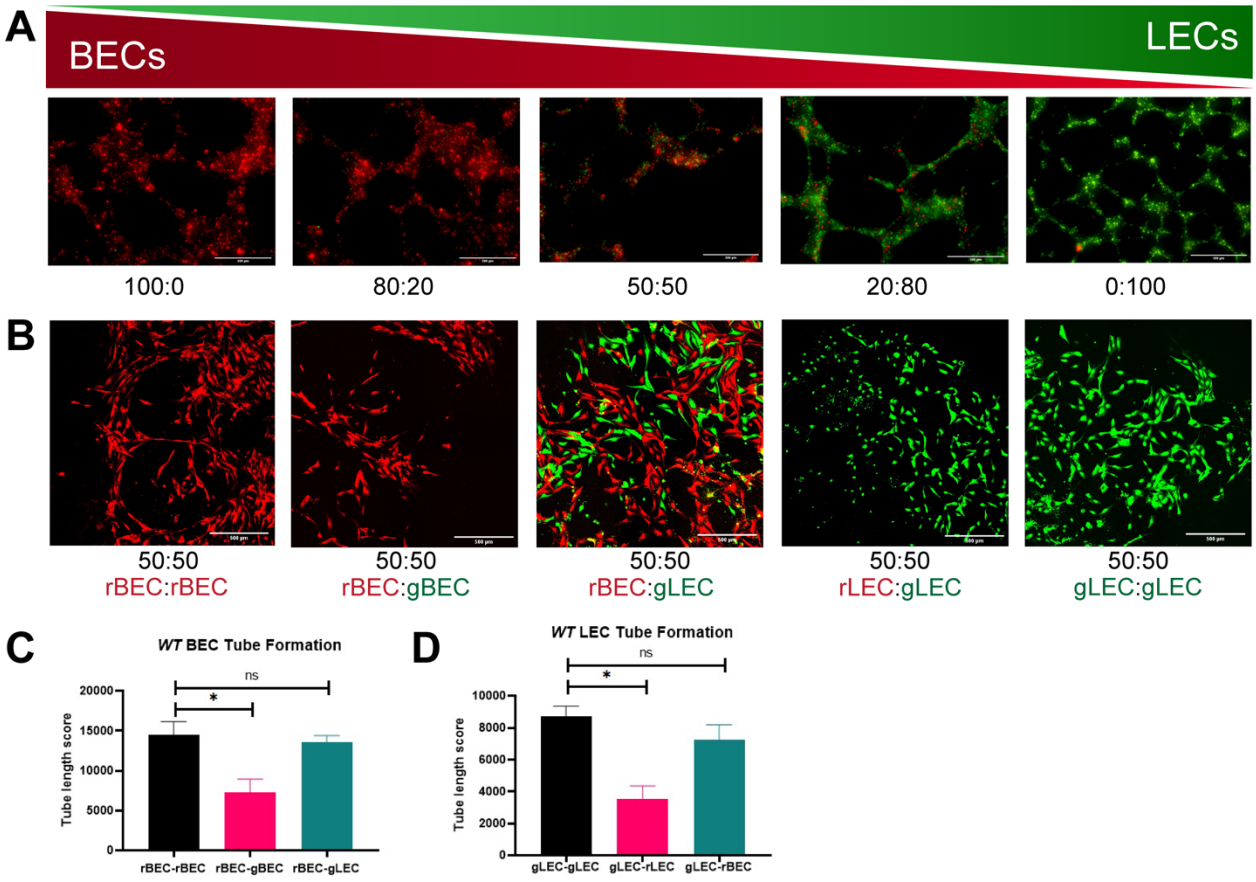

Figure 2. BEC and LEC form distinct cord-like structures on 2D Matrigel and 3D fibrin gel assays. (A) BEC (pre-labeled in pre-labeled in CellTracker™ Red CMTPX) and LEC (pre-labeled in CellTracker™ Green CMFDA) were seeded on 2D Matrigel at ratios of 100:0, 80:20, 50:50, 20:80, and 0:100 (BECs:LECs). Representative images of cord-like structures (CLS) formation were imaged at 12 hrs. Scale bars are 500 μm. **(B)** BEC and LEC were encapsulated in 3D fibrin gel assay. From left to right, red-BEC only, red-BEC and green-BEC (50:50), red-BEC and green-LEC (50:50), red-LEC and green-LEC (50:50), and green-LEC only. Representative images of CLS formation were imaged at 48 hrs. Scale bars are 500 μm. CLS formed on 3D fibrin gel was quantified for tube length using AutoTube for **(C)** BEC and **(D)** LEC. Data represents mean $\pm$ SD, n=4 per group, n.s. $P > 0.05$, $^*P<0.05$. All P values were determined by unpaired t tests.

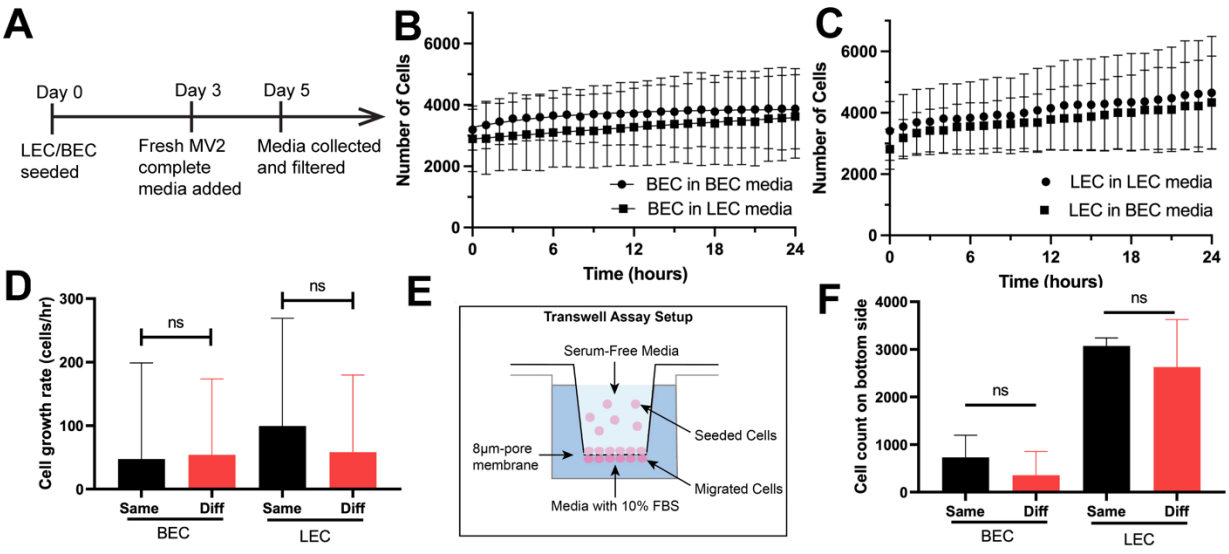

Figure 3. The effects of paracrine signaling on BEC and LEC. (A) A timeline for BEC and LEC-conditioned media collection. Conditioned media were collected after 48 hours of BEC or LEC cultures. Cell proliferation assay with **(B)** BEC and **(C)** LEC using the same (circle data points) and different (square data points) cell line-conditioned media. **(D)** Cell growth rates of BEC and LEC were quantified at 3,500 cells/well using the label-free cell proliferation protocol (Lionheart FX Microscope). Each sample was repeated 12 times. **(E)** A schematic diagram to illustrate the layout of the transwell migration assay. The outer well was filled with conditioned media from either the same or different cell type. **(F)** The top of the membrane was cleaned and imaged on a fluorescence channel to quantify the migrated cells after 24 hours. Each sample was repeated 3 times. Data represents mean ± SD, n=4 per group, n.s. $P > 0.05$, All P values were determined by unpaired t tests.

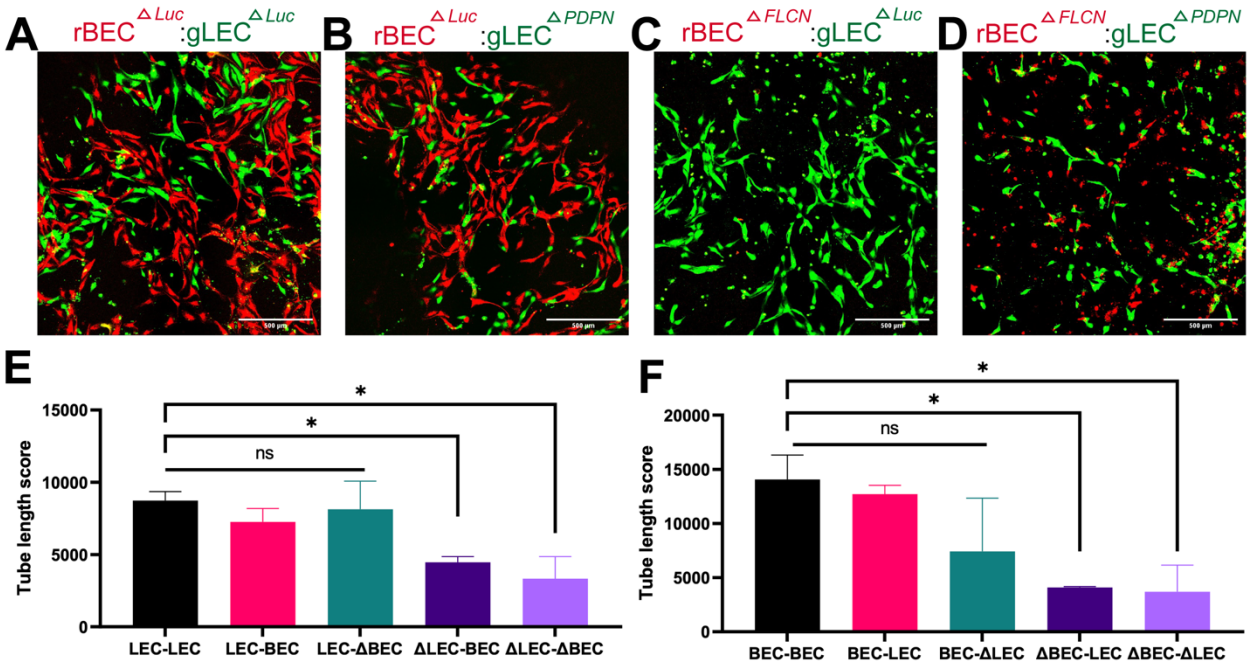

Figure 4. The roles of *FLCN* and *PDPN* on cord-like networks formation. (A and **B)** *Luciferase* knockout BEC (rBEC $^{\Delta Luc}$) or **(C** and **D)** *FLCN* knockout BEC (rBEC$^{\Delta FLCN}$) stained in red are encapsulated in 3D fibrin gels together with **(A** and **C)** *Luciferase* knockout LEC (gLEC $^{\Delta Luc}$) or **(B** and **D)** *PDPN* knockout LEC (rLEC$^{\Delta PDPN}$) stained in green. Representative images of CLS formation were imaged at 48 hrs. Scale bars are 500 μm. **(E** and **F)** CLS formed on 3D fibrin gel was quantified for tube length using AutoTube. Data represents mean $\pm$ SD, n=4 per group, n.s. $P > 0.05$, *$P<0.05$. All P values were determined by unpaired t tests.

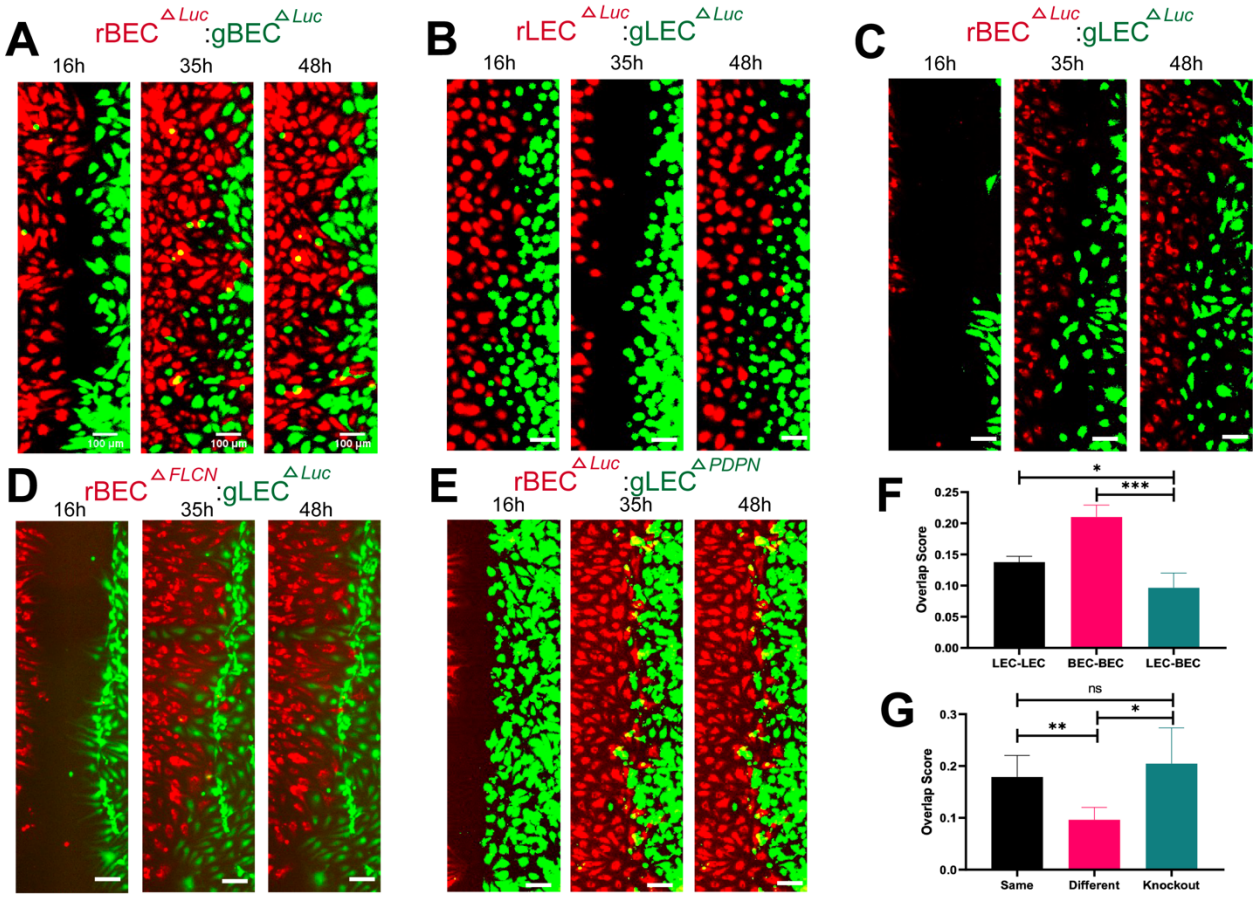

Figure 5. The roles of *FLCN* and *PDPN* on cell migration. Representative images of the wound healing assay taken at t=16, 35, and 48 hours for **(A)** BEC (in *red*) : BEC (in *green*), **(B)** LEC $^{\Delta Luc}$ (in *red*) : LEC $^{\Delta Luc}$ (in *green*), **(C)** BEC $^{\Delta Luc}$ (in *red*) : LEC $^{\Delta Luc}$ (in *green*), **(D)** BEC$^{\Delta FLCN}$ (in *red*) : LEC $^{\Delta Luc}$ (in *green*), and **(E)** BEC$^{\Delta FLCN}$ (in *red*) : LEC $^{\Delta Luc}$ (in *green*). Each well was seeded with 7,000 cells and allowed to settle for 24 hours, then imaged for up to 48 hours. Scale bars are 500 μm. Overlap scores for **(F)** wild-type BEC and LEC, as well as **(G)** knock-out BEC and LEC. The LEC-BEC condition consists of 4 replicates and the same and knockout conditions consist of 4 replicates from either of the two conditions. Data represents mean $\pm$ SD, n=4 per group, n.s. $P > 0.05$, *P<0.05, **P<0.01, and ***P<0.001. All P values were determined by unpaired t tests.